IEEE Access
Multidisciplinary | Rapid Review | Open Access Journal

Received March 13, 2019, accepted April 8, 2019, date of publication April 23, 2019, date of current version May 24, 2019.

Digital Object Identifier 10.1109/ACCESS.2019.2912333

Design and Experiments of Electromagnetic Heating Forming Technology

CHENGXIANG LI, YAN ZHOU, PENGFEI WANG, XIANMIN WANG, SHOULONG DONG, JIAN DU, ZHIGANG LIAO, CHENGUO YAO, (Member, IEEE), JIANWEN TAN, AND YAN MI, (Senior Member, IEEE)

State Key Laboratory of Power Transmission Equipment and System Security and New Technology, School of Electrical Engineering, Chongqing University, Chongqing 400030, China

Corresponding author: Chengxiang Li (lichengxiang@cqu.edu.cn)

This work was supported in part by the National Natural Science Foundation of China under Grant 81501615.

ABSTRACT Electromagnetic forming (EMF) has been widely applied in industries. However, it's still hard to form thick or hard metal work pieces due to the limitation of its system power. Moreover, increasing the input voltage or capacitors may cause the problem of insulation, reduce the lifetime performance of devices, and lead to the cost increase and safety issue. Therefore, this paper proposes a novel technology named electromagnetic heating forming (EMHF), which combines EMF with electromagnetic induction heating (EIH) based on their similar working principles to make it easier to form the thick or hard metal work pieces. The EMHF can reduce the deformation resistance of work pieces by preheating treatment, and produce small discharge energy to deform work pieces. A 5kV/1.68kJ/135μ F EMHF system with a high-current pulse generator and a high-frequency heating source, which consists of an autonomous current-fed push-pull resonant inverter based on a zero voltage switching circuit and a resonant network, has been designed, built, and tested successfully. A finite element model coupling with the electromagnetic field, solid mechanics field, thermal field, and deformed geometry has also been built in COMSOL Multiphysics to analyze the EMHF process. Tube compression EMHF experiments of different input voltages, thicknesses, and temperatures have been carried out. The experimental and simulation results demonstrate that the EMHF can reduce the requirements of the deformation process by preheating treatment, which can't be done by EMF. Besides, the deformation can be controlled by the preheating temperature during the EMHF process. Therefore, the EMHF has great potential in industrial applications.

INDEX TERMS Electromagnetic forming (EMF), electromagnetic induction heating (EIH), electromagnetic heating forming (EMHF) system, pulse generator, inverter.

I. INTRODUCTION

Electromagnetic forming (EMF) is a fast, intelligent and environment-friendly manufacturing technology which has widely been applied in deforming tubular or sheet metal work pieces [1]–[7]. It is a non-contact forming process using Lorentz force caused by the large discharge current flowing through the forming coil. This technology can be explained through Maxwell equations: a time-varying magnetic field produced by the discharge current in the forming coil induces eddy current in the work piece and hence Lorenz force applied on the work piece. As is shown in Fig. 1, the EMF system mainly consists of two parts: a high-current pulse generator and a forming system [2]. The high-current pulse generator consists of the power supply U, capacitor C, charging switch K_1 and discharging switch K_2. The pulse generator works simply. Firstly, the charging switch K_1 is turned on, and the power supply U charges the capacitor C. Then, the charging switch K_1 is turned off and the discharging switch K_2 is turned on. Lastly, the capacitor discharges to the forming coil.

This forming system designed for tubes includes a forming coil and work pieces, as is shown in Fig. 1. Tubes achieve a high velocity to be formed in about $20 - 100\mu$s during the EMF process. The dynamics of this event, including die impact, enhance the formability of tubes and eliminate spring-back of tubes [8]–[13]. Thus, EMF is expected to help overcome some formability barriers that prevent more

The associate editor coordinating the review of this manuscript and approving it for publication was Zhigang Liu.

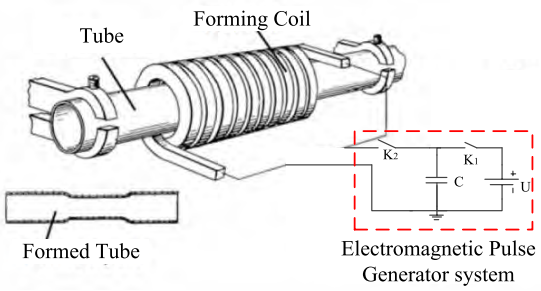

FIGURE 1. Electromagnetic forming system.

widespread use of materials such as aluminum in lightweight structural applications [14]. And this technology has no need to lubricate [15]. It holds prospects of being widely applied, which attracts many scholars' interest. In recent years, scholars have focused on the numerical calculation, circuit optimization, and experimental study of EMF technology. Anter proposed a mathematical and numerical model that captures the pertinent physics and offers exceedingly useful solutions based on the ANSYS which could help engineers to design advanced EMF systems [16]. Ali offered a numerical method which involves circuit analysis, electromagnetic field calculation and the dynamic plastic deformation of the work piece to solve the problem of the electromagnetic forming of clamped thin circular metal sheets by using a flat spiral coil [17]. Besides, some studies have been focused on improving the efficiency of the forming process by optimizing the equipment. Luis proposed a new high-current generator with energy recovery based on two resonant power modules, which improves the efficiency of EMF system by up to 32% and reduces charging time in comparison by 68%, and energy can be maximized by adding more modules [18]. Moghadam proposed a new pulsed power supply system based on Z-source full-bridge inverter that has the flexibility in terms of controlling energy and charging the capacitor to provide a proper pulse for EMF, while there is a voltage limitation resulting from the limited use of semiconductor switches [19].

However, some problems still exist in the process of thicker or harder work pieces forming, which brings higher requirements for the EMF system. That means more energy is needed to produce enough Lorentz force. Improving energy by increasing input voltage and adding capacitors are two most commonly-used methods. Nevertheless, the maximum input voltage and capacitance are fixed when the system is produced. And the methods will also bring about other problems such as insulation strength reducing, bigger EMF volume, shorter service life of trigger vacuum switch (TVS) and capacitors, higher requirements for electrical connection, and cost increase. Higher voltage will also reduce the circuit security and stability. All of those problems limit the EMF's application in many fields. Preheating treatment can improve the plasticity of the metal materials. Therefore, electromagnetic induction heating (EIH) is proposed for reducing the forming conditions in this work because it can provide non-contact, fast, and efficient heating of conductive materials. The preheating treatment is made before the forming process to improve metal atomic energy and plasticity, and reduce deformation resistance. Besides, EIH is becoming one of the preferable heating technologies in industrial [20], domestic [21] and medical applications [22]. Moreover, EMF and EIH have the similar working principle, and the coil can be used to form or heat the work pieces. Thus, EMF and EIH are combined to EMHF to reduce the forming limitations and make the forming requirements easy to be met. Based on the theory of EMHF technology, a novel EMHF system was developed. The tube compression EMHF results are as expected, which proves the high feasibility of the EMHF technology.

The remainder of this manuscript is organized as follows. First, the basic principle and circuit of EMHF is introduced in section II. Then, in section III is presented a description of the EMHF system and tube compression experimental condition, followed by experimental results and analysis in section IV. A simulation based on COMSOL Multiphysics is described in section V. The conclusions of this study and avenues for future work are introduced in last section.

II. BASIC PRINCIPLE AND CIRCUIT OF EMHF

A. THEORETICAL ANALYSIS OF EMHF

The power of an EMF system is related to the input voltage and capacitance according to (1). Increasing the input voltage or capacitance are two effective ways to gain more energy.

$$W = \frac{1}{2}CU^2 \tag{1}$$

where C is the capacitance of energy storage capacitor and U is the input voltage.

The working current flowing in the forming coil discharges from the capacitors and the discharge process is very transient. According to the RLC equivalent circuit, the discharge process of such a system is described by the following equations:

$$\frac{d^2I(t)}{dt^2} + 2\xi\frac{dI(t)}{dt} + \omega_0^2 I(t) = 0 \tag{2}$$

$$\xi = \frac{R}{2L} \tag{3}$$

$$\omega_0 = \sqrt{\frac{1}{LC}} \tag{4}$$

$$\omega_{\mathrm{d}} = \sqrt{\frac{1}{LC} - \left(\frac{R}{2L}\right)^2} \tag{5}$$

where $I(t)$ is the discharge current flowing in the forming coil. ξ is the attenuation coefficient. ω_0 is the resonant angular frequency. R, L, C are the circuit parameters and t is the time. ω_{d} is the oscillation angular frequency.

The discharge current $I(t)$ can be given by solving the equations above.

$$I(t) = -\frac{V_0}{\omega_d L}\exp(-\xi t)\sin(\omega_d t) \tag{6}$$

The basic principle of EMF is that the tube near the forming coil induces a great Lorentz force and is deformed at a high-speed in a short time. Equations (6)-(8) described the Lorentz force during the forming process of EMHF according to [23].

$$\mathbf{f}_m = \mathbf{J}_e \times \mathbf{B} \tag{7}$$

where $\mathbf{f}_m$ is the Lorentz force in the tube. $\mathbf{B}$ is the magnetic flux generated by the discharge current flowing through the coil and $\mathbf{J}_e$ is the induced current density in the tube. Thus, $\mathbf{B}$ and $\mathbf{J}_e$ are both related to the discharge current $I(t)$ which is decided by the input voltage U, the capacitance C, the resistance R and the inductance L.

The displacement equation in the EMF process is given by the following equilibrium equation:

$$\rho\frac{\partial^2 \mathbf{S}}{\partial t^2} - \nabla\cdot\sigma_f = \mathbf{f}_m \tag{8}$$

where $\mathbf{S}$ is the displacement of tube, which can reflect the degree of deformation. ρ is the metal density. σ_f is the flow strength.

To reflect the high strain-rate effect on the mechanical properties of the tube, the flow strength of the tube according to the work from Suzuki [23] is approximated by

$$\sigma_f = K\left(\left(\frac{\sigma_Y}{K}\right)^{1/n} + \varepsilon\right)^n \tag{9}$$

where K is the strength coefficient. n is the strain hardness. σ_Y is the yield stress and it is related to the metal temperature. ε represents the plastic strain.

There are two approaches to improve the deformation effect on tubes according to (5)-(9).

1) The first is improving the input voltage to increase the discharge current. This way can improve the induced current density and the magnetic flux, and can generate greater Lorentz force to overcome the deformation resistance of work pieces.

2) The second is reducing the flow strength of work pieces. Changing the yield stress, strength or strain of the work pieces to reduce the flow strength is another method.

This study chooses the second method and proposes a new technology named EMHF to form thick and hard work piece. The heating source in the EMHF can reduce the yield stress of work piece by raising its temperature.

B. BASED PRINCIPLE OF EIH

Preheating process means putting energy into the work piece. The energy renders the thermal motion of metal atoms more intense and make it easier to go out of their bondage. In other words, atoms with high temperature are easier to move under the same pressure conditions. EIH possesses many advantages such as being fast, controlled, safe, and high-efficient. Thus, it is chosen to decrease the deformation resistance of metal work piece in this study. In addition, EMF and EIH rely on electromagnetic induction principle to affect the work piece. And the coil can be used to form and heat the work piece, so they can be integrated on a system easily.

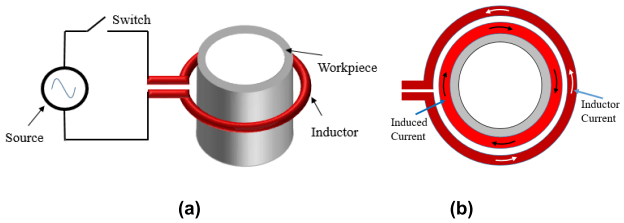

FIGURE 2. Typical arrangement of an EIH system (a) general view and (b) top view.

Figure 2 shows a typical structure of an EIH system [24]–[27]. An alternating current (AC) source is used to supply the alternating current to a coil. The coil generates an alternating magnetic field, in which the heating target, i.e., the work piece, is immersed. Then, there are two physical indicators of the heated work piece: eddy currents and magnetic hysteresis [28]. Eddy currents oppose to the magnetic field applied to the work piece, and they produce heating through Joule effect, which is commonly the main heat source in EIH processes. There are three effects in EIH: proximity effect, skin effect and torus effect. As is showed in Figure 2(b), there are inductor current in forming coil and induced current in the tube. The coil and the tube can be regarded as two parallel wire which flow in the opposite direction. The inductor current and induced current produce the proximity effect, while inductor current is concentrated on the inside surface of the coil. The induced current of the tube is focused on its outer edge.

The working principle of EMF is the similar to that of EIH. However, there are also some differences between them, which are listed here:

1) The EMF current is much stronger than the EIH current;

2) The EMF current has shock waveform while the EIH current has sinusoidal waveform;

3) The frequency of EIH current is different from that of the EMF current.

In the EMHF process, the work piece is preheated while the capacitors are charged. According to Maxwell equations, the induction electric potential of work piece is:

$$e = -N_2\frac{d\phi}{dt} \tag{10}$$

where N_2 is the equivalent number of work piece turns, ϕ is the magnetic flux generated by the time-varying current.

If the magnetic flux ϕ is alternating, assuming that

$$\phi = \phi_M \sin\omega t \tag{11}$$

$$e = -N_2\frac{d\phi}{dt} = -N_2\phi_M\omega\cos\omega t \tag{12}$$

The valid value is given as follows.

$$E = 4.44 f N_2 \phi_M \tag{13}$$

The Joule heat of work piece can be defined as follows.

$$Q = \frac{E^2}{R_l} t \tag{14}$$

where R_l is the resistance of the work piece, t is the preheating time. Thus, the heating temperature can be controlled by the heating time.

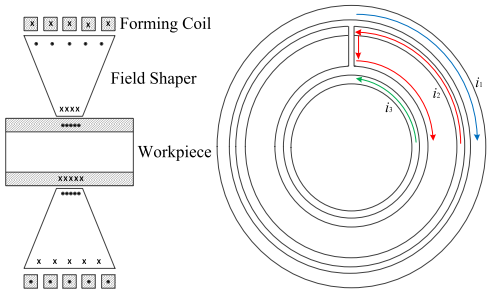

FIGURE 3. The working principle of (a) section view and (b) top view of the field shaper.

Most importantly, field shaper is used to enhance the magnetic field of the EMHF. The working principle of the field shaper is showed in Fig. 3, where i_1 is the preheating current or discharge current in the coil, i_2 is the induced current in the field shaper, and i_3 is the induced current in the work piece. The relationship between i_3 and i_1 is given as follows.

$$i_3 = \eta N_1 i_1 \tag{15}$$

where N_1 is number of coil turns, η is the energy transfer efficiency between the coil and the tube.

Thus, the energy can be concentrated in the forming area by the field shaper when the forming coil is bigger than the work piece.

C. DBASED DIAGRAM OF EMHF SYSTEM

The basic process of EMHF consists of three steps: a high voltage direct-current (DC) power supply charges the capacitor bank and stores energy while preheating the work piece; the discharge switch is triggered and the capacitor bank starts to release energy; the time-varying magnetic field and the induced eddy current are produced, then the work piece is formed by the large Lorentz force.

To better show all of the steps mentioned above, a novel diagram of EMHF system is designed, as is shown in Fig. 4. It mainly consists of a high-current pulse generator, a high-frequency sinusoidal wave generator and a forming system. A high-voltage DC power supply is used to charge the capacitor bank. Concurrently, the high-frequency sinusoidal wave generator based on DC source and inverter heats the tubes by electromagnetic induction before the trigger source is working. Then the FPGA switches off the vacuum relay and

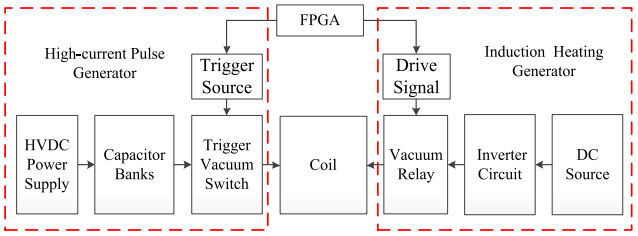

FIGURE 4. The diagram of EMHF system.

triggers the TVS conducted. The capacitor banks release the energy to the coil, producing the high current pulse.

The part of high-current pulse generator works under a high voltage and a large current while induction heating generator is low in working voltage and small in working current. Therefore, the heating source needs to be isolated from the high voltage and the large current. The vacuum relay with a high operation voltage and a large operation current is used to isolate the two parts. Thus, there will be no interactive influence between the forming part and the preheating part.

III. DEVELOPMENT AND ESTABLISHMENT T OF THE EMHF SYSTEM

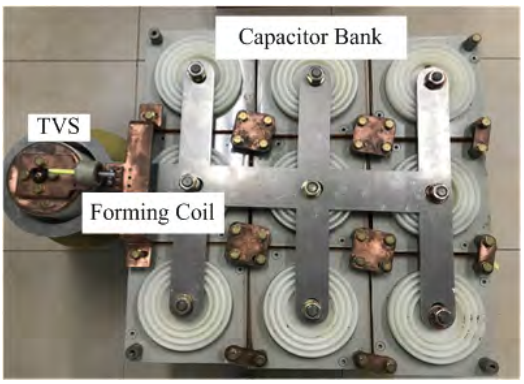

(a)

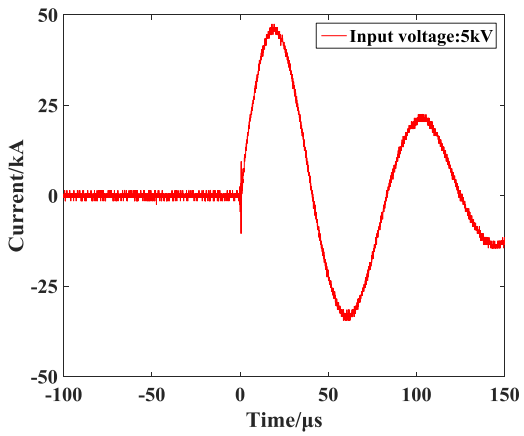

(b)

FIGURE 5. High-current pulse generator and its output waveform (a) High-current pulse generator and (b) The output discharge current.

A. DEVELOPMENT AND ESTABLISHMENT OF THE HIGH-CURRENT PULSE GENERATOR

A 1.68kJ high-current pulse generator with a capacitance of 135μF and a maximum charging voltage of 5kV is designed for tube compression EMHF experiments, which is exhibited in Fig. 5(a). A high-voltage DC power supply is used to charge the capacitor bank. Nine paralleled 15μF pulse capacitors are used to storage energy. The circuit is connected by the aluminum alloy plate, and reduces stray inductance by increasing the cross-sectional area of the plate. This work chose TVS as the discharge switch because of its superior performance. It is connected with the working coil and capacitor bank through the special barrel structure aluminum alloy sleeve. The discharge loop area is designed to be very small to reduce the energy loss. A trigger source is designed and built for the TVS [29], which generates a 5μs/5kV trigger pulse. The discharge current is measured by the Rogowski coil with a sensitive of 50kA/V, as shown in the Fig. 5(b). The maximum value of the discharge current is about 45kA when the input voltage is 5kV.

B. DEVELOPMENT AND ESTABLISHMENT OF THE WORKINF COIL AND FIELD SHAPER

The working coil is an important part in the EMHF system. It is used to produce a time-varying magnetic to heat and form work pieces. The coil is fabricated with rectangular cross-section copper coils because it is mechanically stronger than that fabricated with circular cross-section copper coil [30]. The cross-sectional area of each coil turns is about 7 x 5 mm^2 to ensure enough stiffness. The angle relates to the inductance of field shaper. According to [31], the larger the angle is, the stronger inductance of the field shaper is. Thus, 60 degrees is chosen to increase the inductance, which improves the efficiency of the forming process.

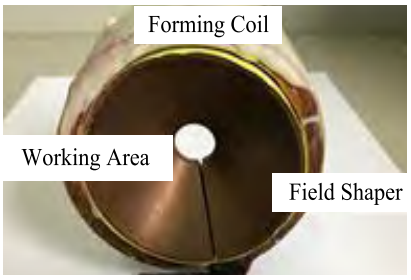

FIGURE 6. Working coil and field shaper.

Figure 6 describes the working coil and the field shaper. The clearance between them is about 0.2 mm and Mara tape is used for insulation. The turns of the coil is 6 and the coil diameter is 100mm. The diameter of the hole is 16.5mm and working area length is about 5mm. The forming coil, field shaper and work piece can be modeled as an equivalent resistor R_{eq} and an equivalent inductor L_{eq}, which is described in Fig. 7.

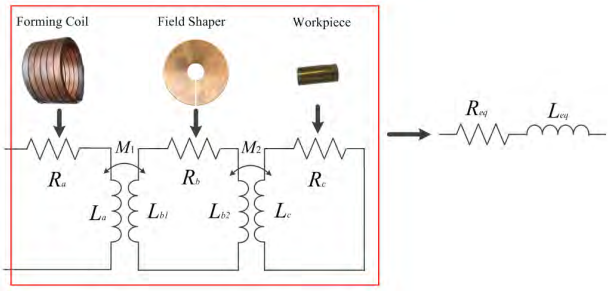

FIGURE 7. Electrical equivalent model of the forming coil, field shaper and work piece.

C. DEVELOPMENT AND ESTABLISHMENT OF THE HIGH FREQUENCY EIH SOURCE

The EIH source with high-frequency is used to preheat the tubes while the capacitor bank is charged. This process mainly includes rectifier and inverter. The alternating magnetic field is produced by the high-frequency current in the forming coil, and then eddy current is produced in the field shapers and work piece. The inverter is the most important one in the EIH source and an autonomous current-fed push-pull resonant inverter is used to convert the direct-current into the high-frequency alternating-current in this study, which can increase the frequency with full resonance and soft switching operation [32].

The schematic diagram of the proposed inverter is presented in Fig. 8. It includes a DC power supply, two large inductors, a zero voltage switching (ZVS) circuit, a resonant network and two MOSFETs used as switches. The equivalent resistor R_{eq} and inductor L_{eq} are connected in parallel in the resonant network. And a tuning capacitor C is added to complete the resonant tank. L_1 and L_2 are about 300μ H according to simulation in the Matlab. C is about 2μF according to calculation.

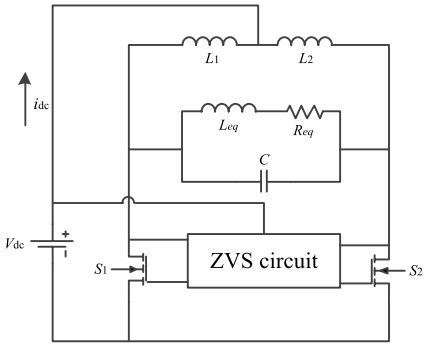

FIGURE 8. The schematic diagram of the EIH Source.

The high-frequency EIH source is described in Fig. 9(a). The AC-DC power supply converts the 220V alternating current into 12V direct current, which provides the energy for the EIH source. The frequency of heating current is set from 60kHz to 110kHz and a protection circuit is designed in the source. The heating source will stop working when the

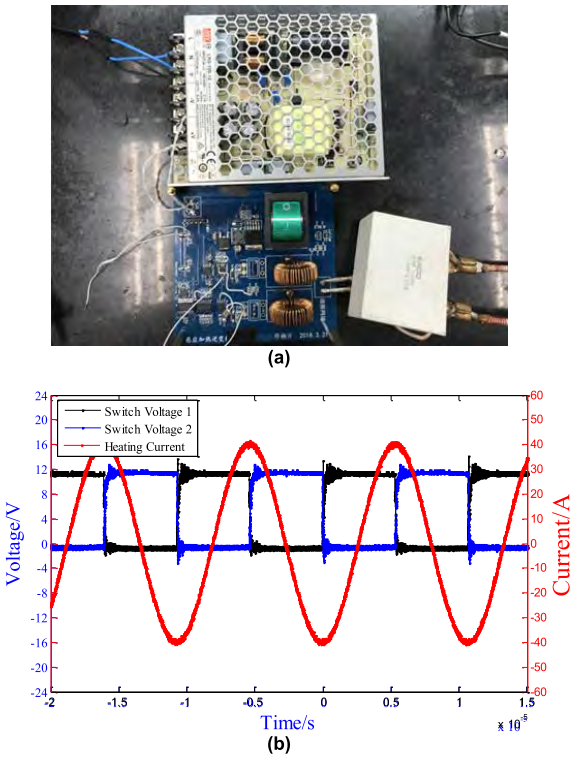

FIGURE 9. High-frequency EIH device (a) EIH device (b) The output waveform of the heating current with 93kHz frequency.

frequency reaches more than 110kHz, which can be regarded as the short circuit phenomenon. Fig. 9(b) shows the output waveform of the heating current and the voltages waveform of the switches. The output current amplitude can be up to 40A, and the frequency is about 93kHz. The valid value of the current is about 28.3A.

Moreover, the skin depth holding influence on the heating effect depends upon the material electrical conductivity, magnetic permeability and EIH device frequency, as is shown by (16)

$$d = \frac{1}{\sqrt{\pi \sigma \mu f}} \tag{16}$$

where the d is the skin depth, f is the frequency of the heating current, the μ represents the magnetic permeability of the tube and σ is the electrical conductivity of the tube.

The resonant frequency f is related to the L_{eq} and C_0, which can change autonomously according to [30]. So materials and thick tubes differ in their frequency and skin depth.

IV. EXPERIMENTAL RESULTS AND ANALYSIS

A. THE SAMPLES AND MEASUEMENT DEVICE

To verify the feasibility of the EMHF, tube compression EMHF experiments were carried out. The 6061 aluminum alloy was selected as the material in the experiments because it has good electrical conductivity and is widely used in the industries. The tube's outer diameter is 16mm and its length is 20mm.

In the EMHF experiments, the preheating temperature is decided by the preheating time and measured by the U5855A TrueIR thermal imager shown in Fig. 10, which is produced by the KEYSIGHT. The U5855A TrueIR thermal imager can produce standard thermal images. Fig. 10 shows the measurement result of the heating process. The temperature distribution is this: the temperature of tube and the part of the field shaper near the tube are the highest, and the temperature of rest part is relatively low. The induced eddy current flowing in the tube is much stronger than the discharge current according to (15). Thus, the Joule heat and the temperature rise of the tube is also larger than that of the forming coil. There are some differences between the theoretical calculation and the actual measurement of preheating temperature in this study, for there is no way to measure the temperature accurately resulting from the good heat conduction of metals. And the highest surface temperature ever measured is regarded as the predetermined temperature. In the experiments, in order to reduce the influence of high temperature on the forming coil, a simple water cooling system consisting of water pipes and water pump is used to cool the forming coil and insulating layer.

FIGURE 10. Temperature measurement diagram.

High-voltage probe P6015A produced by Tektronix is used to measure the voltage of the capacitor bank. And a Rogowski produced by MEATROL is used to measure the discharge current.

B. EFFECT OF DIFFERENT INPUT VOLTAGES AND TEMPERATUREES

The typical forming results of the 6061 aluminum alloy tubes with different input voltages are illustrated in Fig. 11. The tube's thickness is 1mm and its temperature is about 25°C. The input voltages are set to 1kV, 2kV, 3kV, 4kV, 5kV and the input power are about 0.07kJ, 0.27kJ, 0.6kJ, 1.08kJ, 1.68kJ respectively. The deformation results are compared in terms of displacement distance, which are measured by the Vernier caliper.

Figure 11 suggests that the greater the input voltage is, the more obvious the forming result is. The input voltage can affect the discharging current flowing in the forming coil, which produced the induced current density and the magnetic

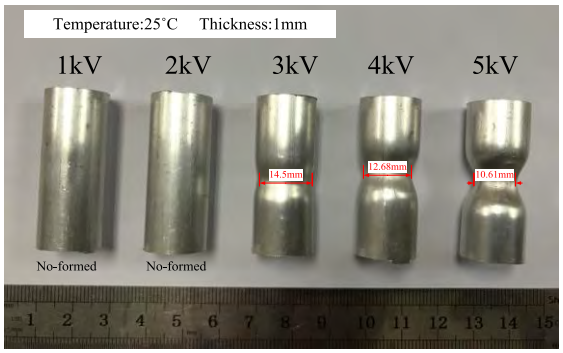

FIGURE 11. The compression forming results of the aluminum alloy tubes with different input voltages.

flux. High voltage will bring more power and produce larger induced current and magnetic flux directly. The Lorenz force will also be strengthened according to (5). So the deformation can be controlled by changing the input voltage. However, the input voltage cannot be infinitely strengthened because it has a limit determined by the operating voltages of the power supply, the capacitor bank, the switches and the circuit. Meanwhile, high input voltage will increase the cost and reduce the life span of the equipment.

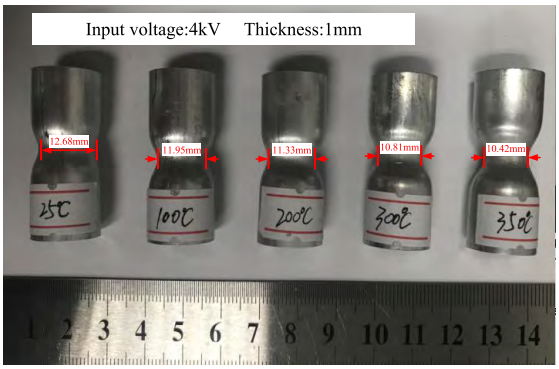

FIGURE 12. The tube compression forming results of deformation under different temperatures.

The typical results of deformation under different temperatures are shown in Fig. 12, when the input voltage is set to 4kV. As the figure shows, the forming effect improves as the preheating temperature increases. The results show that the temperature can change the above problem, and the tube compression result of the 4kV-350°C is better than the 4kV-25°C and 5kV-25°C. That is to say, the effect of low voltage with high temperature can be the same as that of the high voltage with low temperature. So EMHF technology has a lower requirement for the forming process, and the deformation can be controlled by the heating temperature and input voltage. Moreover, the deformation is related to the temperature, and there is no linear relationship between temperature and deformation. This also satisfies the (7)-(9).

C. EFFECT OF DIFFERENT THICKNESSES AND TEMPERATUREES

The typical forming results of aluminum alloy tubes with the different thicknesses under different temperatures are shown in Fig. 13. The thickness of the two tubes are 1mm and 2mm, respectively. And their temperatures are about 25°C and 350°C. The input voltage is 4kV and the input power is about 1.08kJ.

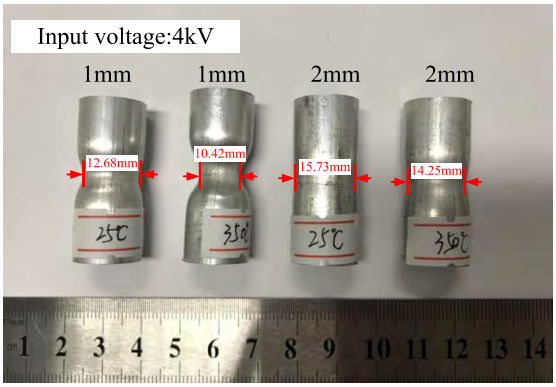

FIGURE 13. The compression forming results of the different thickness aluminum alloy with different temperature.

Figure 13 describes the relationship between the forming result and the thickness under different temperatures. The results demonstrate that the thinner the tube is, the more obvious the forming effect is. Under the same Lorentz force, the deformation of thick tube is little because of its structure, and the deformation resistance of the thick tube is bigger than that of the thin tube. So the thicker tube needs more energy to reduce the deformation resistance. Heating can put enough energy into the tubes to reduce their deformation resistance. Therefore, the thin tube with a high temperature can have the same deformation effect as the thicker tubes. The effect of tube thickness could be reduced by EMHF technology.

V. SIMULATION OF EMHF

A. SIMULATION MODEL IN COMSOL MULTIPHYSICS

EMF is a complex process including electromagnetic field, solid mechanics field and thermal field. The finite element simulation is one of the main methods for physical analysis and COMSOL Multiphysics is a major software used in the analysis of EMF process [33]–[37]. Based on our previous study on EMF process simulation [33] and related references [34]–[37], a finite element model coupling with electromagnetic fields, solid mechanics field, thermal field and deformed geometry was built in COMSOL Multiphysics to analyze the deformation process of tube compression using the EMHF technology.

The geometry model of the tube-compression EMHF simulation is shown in Fig. 14. It consists of the forming coil, tube, field shaper and the solving area. Copper is chosen as the material of the forming coil and field shaper. The tube is made from the 6061 aluminum alloy. The solving area is set

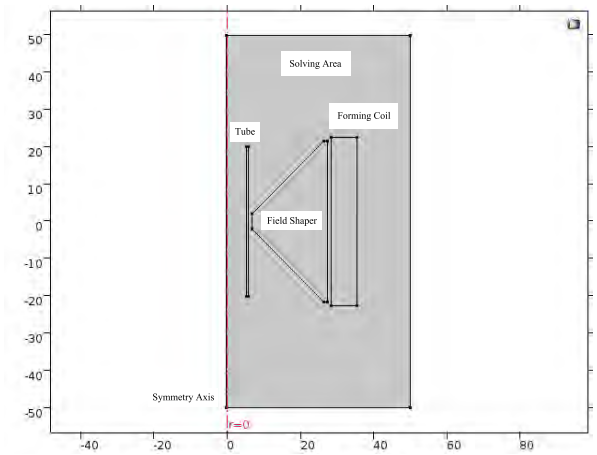

FIGURE 14. 2-D axial symmetry simulation model of tube EMHF.

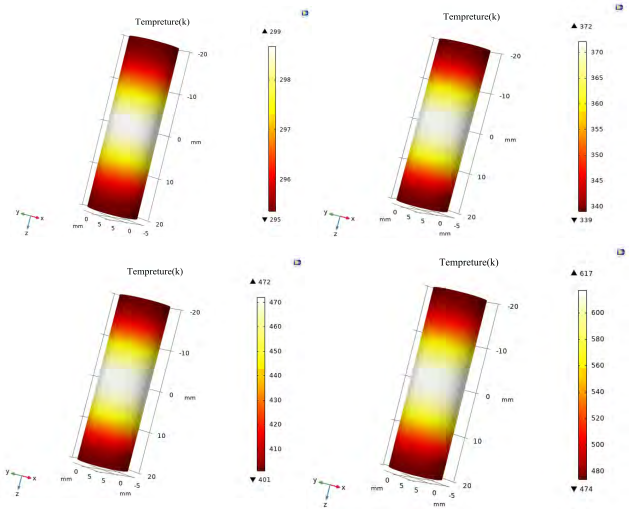

FIGURE 15. The temperature of tube after preheating treatment.

as the air. The aluminum tube is 16mm in its outer diameter of and is 14mm in its inner diameter. The length of the aluminum tube is 40mm. These parameters are consistent with those required by experiments.

However, there are some differences in the simulation steps compared with previous simulation work. The simulation of EIH is carried out firstly, and then forming simulation is carried out. According to [38], the EIH process includes (12)-(14) and (17)-(18) as follows.

$$j\omega\sigma(T)A + \nabla \times \left(\mu^{-1}\nabla \times A\right) = 0 \tag{17}$$

$$\rho C_p \frac{\partial T}{\partial t} - \nabla \cdot k\nabla T = Q(T, A) \tag{18}$$

where ω is the angular frequency and μ is the velocity vector. And A is the magnetic vector potential. ρ is the density of the tube metal. T is the temperature and t is the preheating time. σ is the electrical conductivity. C_p is the specific heat capacity. k is the thermal conductivity. The parameters σ, C_p, and k will be affected by the temperature. Q is the induction heating energy calculated by (14).

TABLE 1. Physical parameters of the tube.

Symbol	Description	Value	Unit
ρ	Density	2.75	g/cm^3
σ_s	Yield strength (20℃)	210	Mpa
K	Strength coefficient	562.5	
n	Strain hardness	0.55	
σ	Conductivity (20℃)	3.7e7	S/m
E	Young's modulus	69	GPa
V	Poisson's ratio	0.33	
μ	Relative permeability	1	
C_p	Specific heat capacity (20℃)	896	J/(Kg*k)
k	Thermal conductivity (20℃)	167	W/(m*K)

The change of magnetic field and Lorentz force is calculated in the electromagnetic field module. Lorentz force can be obtained according to (7). And the change of magnetic field is calculated according to (19)-(21).

$$\nabla \times \mathbf{E} = -\frac{\partial \mathbf{B}}{\partial t} + \nabla \times (\mathbf{V} \times \mathbf{B}) \tag{19}$$

$$\sigma \mathbf{E} = \mathbf{J} \tag{20}$$

$$\mathbf{J}_e = -\sigma \frac{\partial \mathbf{A}}{\partial t} + \sigma \mathbf{V} \times \mathbf{B} \tag{21}$$

where $\mathbf{J}$ is the coil current density. $\mathbf{B}$ is the magnetic flux density. $\mathbf{V}$ is the velocity of the medium. $\mathbf{E}$ is the electric field intensity. $\mathbf{J}_e$ is eddy current density. $\mathbf{A}$ is the magnetic vector potential.

The solid mechanics field is used to simulate the tube-compression process based on (8)-(9).

The physical parameters of the tube is shown in Table 1.

The input excitation source is high frequency sinusoidal current shown in Fig. 9(b) and pulse current shown in Fig. 5(b). The tube will be deformed by Lorentz force in the first rising phase of the discharge current. Therefore, the simulation time of deformation stage is set according to the discharge current waveform.

B. SIMULATION RESULTS AND ANALYSIS

The temperature of tube after preheating treatment in simulation is shown in Fig. 15. The initial temperature is set to 273k. In the simulation, the preheating temperature can be controlled by the preheating time according to (14), and the tubes are preheated to 299k, 372k, 472k and 617k, respectively. As is shown in the figure, the highest temperature area is in the middle of the tube where the working area of the field shaper lies. As the temperature increases, the temperature span extends and the difference of the tube becomes bigger. And there is also temperature difference between the outer and inner of the tube.

The EMHF deformation results of tube under temperature of 299K and 617K are shown in Fig. 16. In order to show the simulation results more clearly, COMSOL Multiphysics software will automatically enlarge display results. The spe-

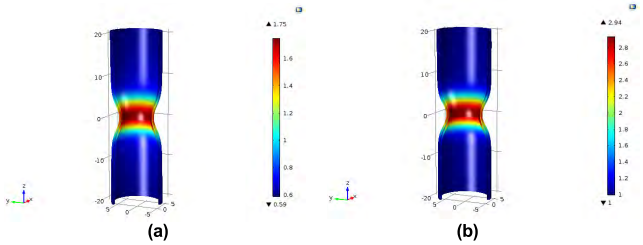

FIGURE 16. The deformation results under different preheating temperatures. (a) Deformation result under the temperature of 299k. (b) Deformation result under the temperature of 617k.

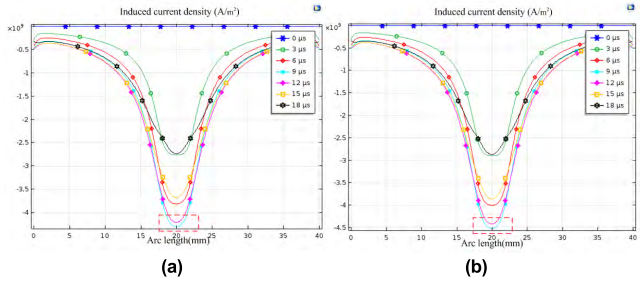

FIGURE 17. The induced current simulation results of the tube at different preheating temperature. (a) Induced current at the temperature of 299k. (b) Induced current at the temperature of 617k.

cific numerical value of the deformation can be seen in the right legend. The deformation of tube is achieved when the input voltage is 4kV. And deformation are concentrated in the working area of field shaper. As is shown in the figure, the radial displacements at the center of the tubes varies with the preheating temperatures. The simulation results can be preliminary evidence that, the temperature will affect the EMF process and EMHF will reduce the limitation of EMF when the input voltage is fixed. In order to explore the feasibility of EMHF, this study also simulated deformation results under different temperature of 372k, 472k and 570k. The displacements of the tube are respectively 2.08mm, 2.46mm and 2.73mm. There are some differences between the experimental results and simulation ones. In the experiment, when the preheating temperature reaches the calculated temperature, the EIH source will be cut off and the pulse current will discharge from the capacitor bank. In the process of capacitor bank discharge, temperature will be reduced and there may be error produced in the measurement process. Meanwhile, the parameters in the simulation are also very ideal. This study conducts qualitative analysis based on the simulation and experimental results, rather than quantitative analysis. Thus, the rule and trends of the simulation results are consistent with the experimental results, which shows that the deformation results improves with the preheating temperature increasing.

The relationship between the temperature rise and the increase of displacement distance is not proportional. The decrease rule of the flow strength with temperature is not the linear according to (9). The temperature not only affects

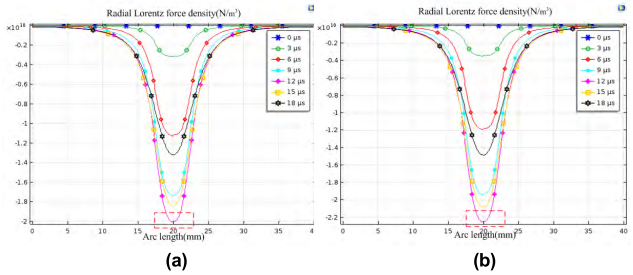

FIGURE 18. The Lorentz force of the tube under different preheating temperatures. (a) Lorentz force under the temperature of 299k. (b) Lorentz force under the temperature of 617k.

the yield strength of tube, but also affects its electrical conductivity. As the preheating temperature increases, electrical conductivity of the tube will decline. The induced current flowing in the tube will be influenced by the change of electrical conductivity. As is shown in Fig.17, the induced current will reduce with the increase of the preheating temperature. And Lorentz force produced by the magnetic field and eddy current will also be influenced. The Lorentz force in the EMHF process is shown in Fig. 18. From the Fig. 18(a) and Fig. 18(b), Lorentz force first increases and then decreases. In the EMHF process, discharge current will increase as is shown in Fig. 5(b). However, the decreases of tube deformation and the internal magnetic flux of the tube lead to the reducing of the induced eddy current. Thus, Lorentz force will decrease. Compared the induced current in Fig. 18(a) with that in Fig. 18(b), Lorentz force will be reduced with the increase of the preheating temperature. Thus, the rising of preheating temperature also has a certain scope. In the simulation results, the tube deformation increases with the rise of the preheating temperature, which shows that the influence of preheating temperature on the yield strength is greater than that on the electrical conductivity.

VI. CONCLUSION

In this study, a developing procedure of EMHF based on EIH and EMF has been presented. And a novel EMHF system of 5kV/135μF was successfully designed, fabricated, and tested. The heating source consists of a DC power supply and an autonomous current-fed push-pull resonant inverter. In addition, the conclusion through the results of tube compression experiments are following.

1) The input power, thickness, and temperature all have influence on the EMF effect. This study firstly chose the rising temperature to improve the compression forming effect instead of increasing the input voltage. When the maximum input voltage and maximum capacitance of the EMHF equipment are fixed, work piece can also be formed by preheating to the proper temperature. And the thick work piece can be formed by a lower input voltage.
2) Preheating process can improve the plasticity and reduce the limitation of work piece, which render the

forming process easier to be completed. The deformation result can be controlled by the suitable temperature, which is related to the preheating time. The cost and volume of the EMF may be changed because high voltage is no longer needed.

3) High preheating temperature will affect the electrical conductivity of work piece, which affects Lorentz force. How to balance the influence of temperature on the yield strength and electric conductivity also needs further research.

REFERENCES

[1] A. G. Mamalis, D. E. Manolakos, A. G. Klada, and A. K. Koumoutsos, "Electromagnetic forming and powder processing: Trends and developments," *Appl. Mech. Rev.*, vol. 57, no. 4, pp. 299–324, Oct. 2004.

[2] V. Psyk, D. Risch, B. L. Kinsey, A. E. Tekkaya, and M. Kleiner "Electromagnetic forming—A review," *J. Mater. Process. Technol.*, vol. 211, no. 5, pp. 787–829, May 2011.

[3] S. H. Lee and D. N. Lee, "A finite element analysis of electromagnetic forming for tube expansion," *J. Eng. Mater. Technol.*, vol. 116, no. 2, pp. 250–254, Apr. 1994.

[4] H. M. Lee, B. S. Kang, and J. Kim, "Development of sheet metal forming apparatus using electromagnetic Lorentz force," *Trans. Mater. Process.*, vol. 19, no. 1, pp. 38–43, 2010.

[5] Y.-Y. Chu and R.-S. Lee, "Effect of field shaper geometry on the Lorentz force for electromagnetic sheet impact forming process," *Proc. Inst. Mech. Eng. B, Manage. Eng. Manuf.*, vol. 227, no. 2, pp. 324–332, Feb. 2013.

[6] J. Li, L. Li, M. Wan, H. Yu, and L. Liu, "Innovation applications of electromagnetic forming and its fundamental problems," *Procedia Manuf.*, vol. 15, pp. 14–30, 2018.

[7] H. Yu, J. Chen, W. Liu, H. Yin, and C. Li, "Electromagnetic forming of aluminum circular tubes into square tubes: Experiment and numerical simulation," *J. Manuf. Processes*, vol. 31, pp. 613–623, Jan. 2018.

[8] M. Seth, V. J. Vohnout, and D. S. Glenn, "Formability of steel sheet in high velocity impact," *J. Mater. Process. Technol.*, vol. 168, no. 3, pp. 390–400, Oct. 2005.

[9] S. F. Golovashchenko, "Springback calibration using pulsed electromagnetic field," *AIP Conf. Proc.*, vol. 778, no. 1, p. 778, Aug. 2005.

[10] E. Iriondo, B. Gonzalez, and M. Gutierrez, "Electromagnetic springback reshaping," in *Proc. 2nd Int. Conf. High Speed Forming*, 2006.

[11] L. Qiu *et al.*, "Analysis of electromagnetic force and experiments in electromagnetic forming with local loading," *Int. J. Appl. Electromagn. Mech.*, pp. 1–9, 2018.

[12] E. Paese, M. Geier, R. P. Homrich, P. Rosa, and R. Rossi, "Sheet metal electromagnetic forming using a flat spiral coil: Experiments, modeling, and validation," *J. Mater. Process. Technol.*, vol. 263, pp. 408–422, Jan. 2019.

[13] Z. P. Lai *et al.* "Application of electromagnetic forming as a light-weight manufacturing method for large scale sheet metal parts," in *Proc. 8th Int. Conf. High Speed Forming*, Columbus, OH, USA. May 2018.

[14] G. K. Fenton and G. S. Daehn, "Modeling of electromagnetically formed sheet metal," *J. Mater. Process. Technol.*, vol. 75, nos. 1–3, pp. 6–16, Mar. 1998.

[15] R. Otin, R. Mendez, and O. Fruitos, "Electromagnetic metal forming," 5rd ed. Barcelona, Spain: CIMNE, 2011.

[16] A. El-Azab, M. Garnich, and A. Kapoor, "Modeling of the electromagnetic forming of sheet metals: State-of-the-art and future needs," *J. Mater. Process. Technol.*, vol. 142, no. 3, pp. 744–754, Dec. 2003.

[17] A. Meriched, M. Féliachi, and H. Mohellebi, "Electromagnetic forming of thin metal sheets," *IEEE Trans. Mag.*, vol. 36, no. 4, pp. 1808–1811, Jul. 2000.

[18] L. M. Redondo, T. Jorge, and M. T. Pereira, "Modular high-current generator for electromagnetic forming with energy recovery," *IEEE Trans. Plasma Sci.*, vol. 42, no. 10, pp. 3043–3047, Oct. 2014.

[19] N. Karimipoor, S. A. Moghadam, A. Yazdian, and M. Mohamadian, "A new pulsed power supply configuration for electromagnetic forming application," in *Proc. 8th Power Electron., Drive Syst. Technol. Conf. (PEDSTC)*, Feb. 2017, pp. 276–281.

[20] M. G. Lozinskii, *Industrial Applications of Induction Heating*, 1st ed. New York, NY, USA: Pergamon, 1969.

[21] W. C. Moreland, "The induction range: Its performance and its development problems," *IEEE Trans. Ind. Appl.*, vol. IA-9, no. 1, pp. 81–85, Jan. 1973. doi: 10.1109/TIA.1973.349892.

[22] P. R. Stauffer, T. C. Cetas, and R. C. Jones, "Magnetic induction heating of ferromagnetic implants for inducing localized hyperthermia in deep-seated tumors," *IEEE Trans. Biomed. Eng.*, vol. BME-31, no. 2, pp. 235–251, Feb. 1984.

[23] Q. Cao *et al.*, "Dynamic analysis of electromagnetic sheet metal forming process using finite element method," *Int. J. Adv. Manuf. Technol.*, vol. 74, nos. 1–4, pp. 361–368, Sep. 2014.

[24] H. Suzuki, H. Negishi, Y. Yokouchi, and M. Murata, "Free expansion of tube under magnetic pressure," *J. Jpn. Soc. Technol. Plasticity*, vol. 27, no. 310, pp. 1254–1260, 1986.

[25] G. H. Brown, C. N. Hoyler, and R. A. Bierwirth, "Theory and application of radio-frequency heating," in *Theory and Application of Radio-Frequency Heating*. 1947.

[26] J. W. Cable, "Induction and dielectric heating," *Electr. Eng.*, vol. 67, no. 9, p. 847, Sep. 1948.

[27] V. Rudnev, D. Loveless, R. L. Cook, and M. Black, *Handbook of Induction Heating*. Boca Raton, FL, USA: CRC Press, 2017.

[28] J. Davies, *Conduction and Induction Heating*, no. 11. Stevenage, U.K.: Peregrinus, 1990.

[29] Y. Zhou *et al.*, "Fast-rise-time trigger source based on solid-state switch and pulse transformer for triggered vacuum switch," *IEEE Trans. Dielectr. Electr. Insul.*, vol. 24, no. 4, pp. 2105–2114, Sep. 2017.

[30] S. Mishra, S. K. Sharma, S. Kumar, K. Sagar, M. Meena, and M. Shyam, "40 kJ magnetic pulse welding system for expansion welding of aluminium 6061 tube," *J. Mater. Proc. Technol.*, vol. 240, pp. 168–175, Feb. 2017.

[31] Z. Zhao, "Research on magnetic pulse joining of 3A21 aluminum-20 steel tubes with filed shaper assisted coil," Ph.D. dissertation, School Mater. Sci. Eng., Harbin Inst. Technol., Harbin, China, 2011.

[32] A. Abdolkhani and A. P. Hu, "Improved autonomous current-fed push-pull resonant inverter," *IET Power Electron.*, vol. 7, no. 8, pp. 2103–2110, Aug. 2014.

[33] Y. Zhou *et al.*, "Finite-element simulation and experiments on plastic heating in the process of electromagnetic pulse forming," *IEEE Trans. Plasma Sci.*, vol. 46, no. 10, pp. 3427–3437, Oct. 2018.

[34] S. Dond, H. Choudhary, T. Kolge, and A. Sharma, "Analysis of the variation of the discharge circuit parameters during electromagnetic forming processes," *Int. J. Precis. Eng. Manuf.*, vol. 20, no. 3, pp. 375–382, Mar. 2019.

[35] L. Qiu *et al.*, "Analysis of electromagnetic force and deformation behavior in electromagnetic tube expansion with concave coil based on finite element method," *IEEE Trans. Appl. Supercond.*, vol. 28, no. 3, Apr. 2018, Art. no. 0600705.

[36] J. Wu, L. Qiu, Q. Chen, Q. Cao, and X. Han, "Research of thermal loads in plate forming coil during repeated electromagnetic forming process," in *Proc. IEEE Int. Instrum. Meas. Technol. Conf. (I2MTC)*, May 2018, pp. 1–5.

[37] Q. Cao *et al.*, "Analysis and reduction of coil temperature rise in electromagnetic forming," *J. Mater. Process. Technol.*, vol. 225, pp. 185–194, Nov. 2015.

[38] Y. He, W. Ma, G. Lv, Y. Zhang, Y. Lei, and X. Yang, "An efficient method to separate silicon from high-silicon aluminum alloy melts by electromagnetic directional solidification," *J. Cleaner Prod.*, vol. 185, no. 1, pp. 389–398, Jun. 2018.

CHENGXIANG LI was born in Taian, Shandong, China, in 1979. He received the B.S., M.S., and Ph.D. degrees in electrical engineering from Chongqing University, Chongqing, China, in 2002, 2005, and 2011, respectively, where he is currently a Vice Professor with the College of Electrical Engineering.

His research areas include electromagnetic pulse forming and welding, pulse generation, online monitoring of electrical equipment, insulation fault diagnosis technology, and new technology of electrical engineering in biomedicine and its treatment apparatus.

Dr. Li was a recipient of the Chongqing Technical Invention Third Prize, in 2017.

YAN ZHOU was born in Zhongxian, Chongqing, China, in 1992. He received the B.S. degree in electrical engineering from Chongqing University, Chongqing, China, in 2015, where he is currently pursuing the Ph.D. degree in electrical engineering.

His areas of research include pulse power technology, electromagnetic pulse forming and welding technology, and new technology of electrical engineering in biomedicine and its treatment apparatus.

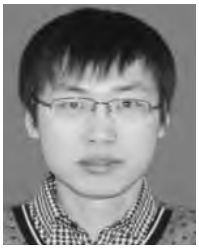

PENGFEI WANG was born in Shenmu, Shanxi, China, in 1987. He received the B.S. and M.S. degrees in optoelectronic engineering from Chongqing University, Chongqing, China, in 2010 and 2013, respectively, where he is currently an Engineer.

His areas of research include pulse power technology, electromagnetic pulse forming, and welding technology.

XIANMIN WANG was born in Kunming, Yunnan, China, in 1995. He received the B.S. degree in electrical engineering from Chongqing University, Chongqing, China, in 2017, where he is currently pursuing the M.S. degree in electrical engineering.

His areas of research include electromagnetic pulse forming and welding.

SHOULONG DONG was born in Taian, Shandong, China, in 1989. He received the B.S. and Ph.D. degrees in electrical engineering from Chongqing University, Chongqing, China, in 2011 and 2017, respectively, where he is currently holding the postdoctoral position.

His areas of research include pulse power technology, and new technology of electrical engineering in biomedicine and its treatment apparatus.

JIAN DU was born in Mianzhu, Sichuan, China, in 1994. He received the B.S. degree in electrical engineering from Chongqing University, Chongqing, China, where he is currently pursuing the M.S. degree.

His areas of research include pulse power technology, electromagnetic pulse forming and welding technology, online monitoring of insulation condition, and insulation fault diagnosis for HV apparatus.

ZHIGANG LIAO was born in Fengdu, Chongqing, China, in 1996. He received the B.S. degree in electrical engineering from Chongqing University, Chongqing, China, in 2018, where he is currently pursuing the M.S. degree in electrical engineering.

His areas of research include pulse power technology, electromagnetic pulse forming, and welding.

CHENGUO YAO (M'08) was born in Nanchong, Sichuan, China, in 1975. He received the B.S., M.S., and Ph.D. degrees in electrical engineering from Chongqing University, Chongqing, China, in 1997, 2000, and 2003, respectively.

He became a Professor with the School of Electrical Engineering, Chongqing University, in 2007. His current works include pulsed power technology and its application in biomedical engineering, online monitoring of insulation condition, and insulation fault diagnosis for HV apparatus.

Dr. Yao received the Chongqing Technical Invention Third Prize, in 2017.

JIANWEN TAN was born in China, in 1980. He received the B.S. and M.S. degrees in electrical engineering from the Science and Technology University of PLA, Nanjing, China, and the Ph.D. degree in electrical engineering from Chongqing University, China, in 2012, where he is doing his postdoctoral research works.

His research interests are in the field of pulse power, power electronics, electromagnetic compatibility, and new electrical technology of biomedical.

YAN MI (M'11–SM'16) was born in Yueyang, China, in 1978. He received the B.S., M.S., and Ph.D. degrees in electrical engineering from Chongqing University, Chongqing, China, in 2000, 2003, and 2009, respectively, where he is currently a Professor with the School of Electrical Engineering.

His current research interest includes the pulsed power technology and its application in biomedical engineering.